Title

Investigation on lateral resolution of surface slope profilers

Authors

Yashchuk, Valeriy V
Lacey, Ian
Arnold, Thomas
et al.

Publication Date

2019-09-09

DOI

10.1117/12.2539527

Peer reviewed

Investigation on lateral resolution of surface slope profilers

Valeriy V. Yashchuk,*[a] Ian Lacey,[a] Thomas Arnold,[b,c] Hendrik Paetzelt,[b] Simon Rochester,[d] Frank Siewert,[e] and Peter Z. Takacs[f]

[a]Lawrence Berkeley National Laboratory, 1 Cyclotron Rd., Berkeley, CA 94720, USA; [b]Leibniz Institute of Surface Engineering (IOM), Permoserstr. 15, 04318 Leipzig, Germany; [c]Technische Universitaet Dresden, 01062 Dresden, Germany; [d]Rochester Scientific, LLC, 2041 Tapscott Avenue, El Cerrito, CA 94530, USA; [e]Helmholtz Zentrum Berlin für Materialien und Energie, Department of Optics and Beamlines, Albert-Einstein-Str. 15, 12489 Berlin, Germany; [f]Surface Metrology Solutions, LLC, 19 South First Street, B-901, Minneapolis, MN 55401, USA

ABSTRACT

We investigate and compare the spatial (lateral) resolution, or more generally, the instrument's transfer function (ITF) of surface slope measuring profilometers of two different types that are commonly used for high accuracy characterization of x-ray optics at the long-spatial-wavelength range. These are an autocollimator based profiler, Optical Surface Measuring System (OSMS), and a long trace profiler, LTP-II, both available at the Advanced Light Source (ALS) X-Ray Optics Lab (XROL). In the OSMS, an ELCOMAT-3000 electronic auto-collimator, vertically mounted to the translation carriage and equipped with an aperture of 2.5 mm diameter, is scanned along the surface under test. The LTP-II ITF has been measured for two different configurations, a classical two-beam pencil-beam-interferometry and a single-Gaussian-beam deflectometry. For the ITF calibration, we apply a recently developed method based on test surfaces with one-dimensional (1D) linear chirped height profiles of constant slope amplitude. Analytical expressions for the ITFs, empirically deduced based on the experimental results, are presented. We also discuss the application of the results of the ITF measurements and modeling to improve the surface slope metrology with state-of-the-art x-ray mirrors. This work was supported by the U. S. Department of Energy under contract number DE-AC02-05CH11231.

Keywords: synchrotron radiation, spatial resolution, point spread function, PSF, instrument's transfer function, ITF, calibration, metrology of x-ray optics, surface metrology, slope profilometry

1. INTRODUCTION

Beamlines at fully coherent free electron laser (FEL) and diffraction limited synchrotron storage ring (DLSR) sources of x-rays, such as the ALS-U (an ongoing upgrade of the Advanced Light Source (ALS) at Berkeley Lab [1,2]), require high-performing, near-perfect, x-ray optics, capable of delivering light to experiments without significant degradation of brightness and coherence. Driven by the desired beamline performance under specific experimental conditions, the specification of surface tolerances of the optics is based on rigorous optical simulations, involving the surface height deviations over the beamline specific spatial frequency range of many orders on magnitude (see, for example, Refs. [3-6] and references therein). It is challenging to reduce these specifications to root-mean-square (RMS) or peak-to-valley (PV) numbers across general length scales (optic manufactures still typically use such single numbers), except as a guide based on current understanding, including the tolerances required by similar beamlines. In the optic's tangential direction, these reduced tolerances can be expressed via the residual (after subtraction of an ideal shape) shape errors of 50–100 nrad (RMS) in the slope domain and 1–2 nm (PV) in the height domain, with tight control of the allowed power spectral density (PSD) and error correlation lengths. In addition, some beamlines require nano-focusing optics with significant tangential and sagittal curvatures; some may require meter-scale mirror lengths [7].

In order to ensure the optimal usage of the super-high-quality optics at beamlines, the dedicated ex situ metrology tools have to be capable of surface measurements over whole spatial frequency range (from the lowest frequency of ~ 10^{-3} mm,$^{-1}$ determined by the mirror length, and up to the ~ 10^{3} mm^{-1}) with high accuracy and reliability. Ideally, metrology accuracy has to be better than the specification by a factor of few (2–5).

*VVYashchuk@lbl.gov; phone 1 510 495-2592; fax 1 710 486-7696; https://als.lbl.gov/people/valeriy-yashchuk/

Multiple tools are used to characterize optics, and no single tool operates with the required accuracy covering the entire range of spatial frequencies. Thus, in the ALS X-Ray Optics Laboratory (XROL) [8,9], slope profilometers and Fizeau interferometers, phase-shifting interferometric microscopes, and atomic force microscopes cover the long, middle, and short spatial wavelength ranges, respectively. For extraction of an complete surface topography of the surface under test (SUT), needed for optical beamline performance evaluations, the measurements with different metrology tools have to be cross-checked and composed (stitched) together. Besides the measurement accuracy of each tool, the stitching reliability suffers on the peculiarity of the tool's spatial frequency response, limiting its resolution.

In this paper, we investigate and compare the spatial (lateral) resolution, or more generally, the instrument's point spread function (PSF) and instrument's transfer function (ITF; defined as the Fourier transform of the PSF) [10-12] of surface slope profilometers of two different types that are commonly used for high accuracy characterization of x-ray optics in the low-spatial-frequency range. These are the upgraded Long Trace Profiler (LTP-II) [13-17] and the autocollimator (AC) based Optical Surface Measuring System (OSMS) [18-21], available at the ALS XROL (see Sec. 2). Both the LTP-II and OSMS essentially operate as high precision deflection sensors to measure angle. These tools have proven capable of characterizing modern aspherical x-ray optics with accuracy of the level of 50-100 nrad (RMS). The LTP-II ITF has been measured for two different configurations, as a classical two-beam pencil-beam-interferometer (PBI) and as a single-Gaussian-beam (SGB) deflectometer (Sec. 3). For the ITF calibration, we apply a recently developed method based on test surfaces with one-dimensional (1D) linear chirped height profiles of constant slope amplitude [22,23]. In Sec. 4, the measured ITF of the LTP-II is compared with that of the OSMS equipped with a light beam aperture of circular orifice of 2.5-mm diameter [21]. Application of the measured ITF to approve the surface slope metrology with the LTP is discussed in Sec. 5. The paper concludes (Sec. 6) by summarizing the main concepts discussed through the paper and outlining a plan for future work.

2. SURFACE SLOPE PROFILOMETRY AVAILABLE AT THE ALS XROL

In this Section, we briefly describe the surface slope profilers, the LTP-II [13-17] and OSMS [18-21], performance of which we treat throughout this paper in the spatial frequency domain.

2.1 The upgraded ALS LTP-II

The LTP-II optical sensor is based on the pencil beam interferometer, initially suggested and patented by K. Von Bieren in 1985 [24-26] and firstly applied in long trace profilers for precision characterization of x-ray mirror surface slope topography in 1986 [27,28]. Having a number of important modifications to the optical schematic [29-31], LTP type profilers remain one of only two classes of surface slope measuring tools that are broadly in use at metrology laboratories of x-ray facilities [14-17,32-43].

Figure 1 shows the current optical schematic of the ALS XROL LTP-II [17] and the LTP-II experimental arrangement used for measurements with the chirped test sample.

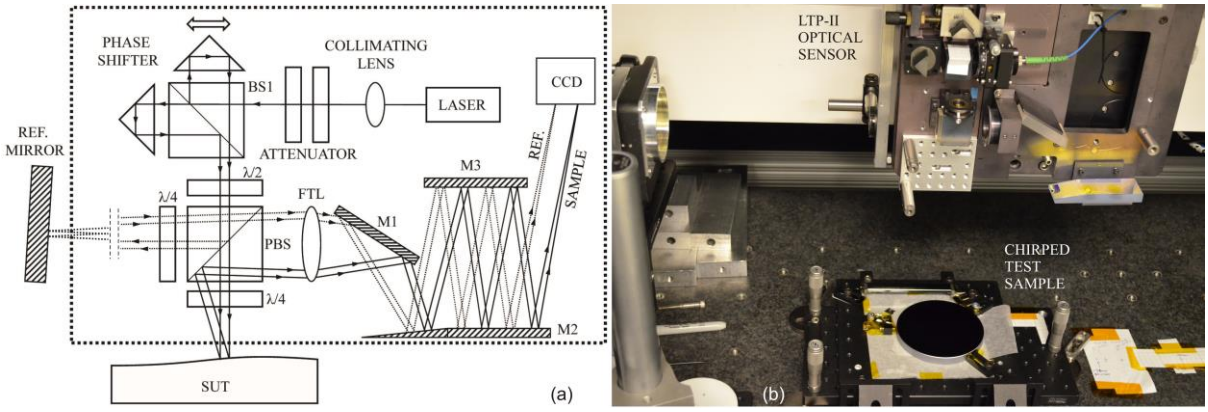

Figure 1. (a) Optical schematic of the ALS XROL LTP-II [17] and the LTP-II arrangement for measurements with the chirped test sample [22,23].

The LTP-II sensor, with elements within the dotted box in Fig. 1(a), is placed on an air-bearing translation carriage. Unlike the last upgrade described in Ref. [17], when we removed the Dove prism in the reference channel, now the

LTP-II is equipped with a single-mode fiber-coupled laser system. This allows us, in particular, to measure diffraction gratings in the manner discussed in Refs. [34,41,42].

The phase shifter [Fig. 1(a)], consisting of the movable and stationary Porro prisms, is used to adjust the phase difference and spatial separation of the two beam components, formed with a beam splitter BS1 [Fig. 1(a)]. The polarizing beam splitter BS2 sends the two-component beams to the SUT (the sample arm) and to the stationary reference mirror (the reference arm). The reference arm records the spurious slope variation due to the carriage pitch wobbling, as well as pointing instability of the laser beam.

In the original ALS LTP-II design [13-16], the Dove prism was used in the reference arm in order to combine with a correct relative sign the errors due to the carriage pitch wobbling and laser beam pointing instability [31]. However, as it was pointed out in Ref. [17], the poor quality of the Dove prism appeared to be one of the major sources of systematic errors. Thus, the Dove prism was removed, assuming that the pointing instability is significantly suppressed in a multi-scan run, arranged according to the optimal scanning strategy, designed to defeat the measurement errors due to instrumental temporal drifts [44]. This assumption has even more sense with the new single-mode fiber-coupled laser system, with extremely small and slow pointing drift. Figure 2 illustrates the point with the results of the LTP-II stability run with a fake motor (no carriage translation) and the reference mirror mounted to the carriage.

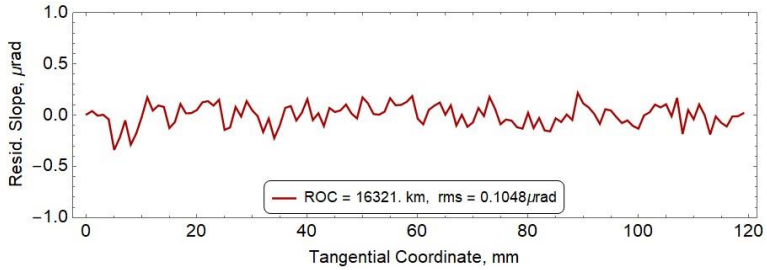

Figure 2. Pointing stability of the LTP-II with the new single-mode fiber-coupled laser system. The LTP-II stability run of 8 scans, optimally arranged to suppress the drift error [44], was performed with a fake motor (no carriage translation) and the reference mirror mounted to the carriage. The major source of the random error is air convection in the reference-beam optical path.

The reflected sample and reference beams are focused with the Fourier transform lens (FTL) to a position sensitive CCD detector. The detected intensity distribution resulting from the interference of the two components of each beam, depends on the phase shift between the beam components. In the classical PBI, with the phase difference adjusted to π, the interference has a destructive character with the intensity minimum in the center. The position of the central minimum is a measure of the SUT surface slope. The folding mirrors, M1, M2, and M3, are used to make a compact design at the FTL focal length of 1.25 m.

The current design of our LTP-II allows us to change the profiler configuration to realize the SGB operation mode by simply placing a beam-stop between the BS1 and the top Porro prism. Due to its relative simplicity (fewer optical elements and, potentially, higher temporal stability), the SGB mode seems to be preferable for high precision measurements with x-ray optics (see, for example, Ref. [38]). However, the questions about possible advantages of the PBI mode are still open. We see two fundamental properties limiting the profiler's performance, which need to be investigated.

One property is the systematic errors of the slope profiler in the PBI and SGB modes of operation. At first glance, due to the inherent differential character of the PBI-based sensor, such a tool should be less sensitive to the imperfections of the sensor optical elements. This question has been empirically investigated in a recent article [16], where a 4-peak mode of operation for the PBI-based LTP was first suggested and experimentally tested. It has been demonstrated that a significant suppression of the LTP systematic error is achievable when the surface slope trace is measured from an average of the two slope traces determined by the left and right side minimums. This observation is still wanting for a comprehensive understanding.

The other fundamental property of a slope profiler is the lateral resolution, described with the instrument's transfer function of the profiler. Comparison of the ITFs of the LTP-II in the PBI and SGB modes of operation is one of the major goals of the present investigation (see Sec. 3).

2.2 The ALS OSMS

The OSMS, recently brought to full scale operation at the ALS XROL [18-21], is a surface slope profiler based on an electronic autocollimator ELCOMAT-3000 [45]. The same ACs are used as optical slope sensors in the so-called Nanometer Optical Measuring Machine (NOM), originally developed at the HZB/BESSY-II [46-48]. A large number of optical metrology labs, including the labs at synchrotron and free-electron-laser x-ray facilities have AC-based profilometers in different arrangements [49-58].

In the arrangement of a classical NOM-like profiler, the AC is placed stationary, while in the course of scanning, a high quality pentaprism (preferably, made of two mirrors [59,60]) is translated along the SUT. In this arrangement, first suggested in Ref. [61], the measurements are insensitive to the systematic error due to carriage wobble. However, because of a strong variation of the distance between the AC and the SUT, it is practically impossible to correct the AC systematic errors by using an angular calibration performed at a single fixed distance [62].

In the ALS OSMS, an ELCOMAT-3000 electronic auto-collimator, vertically mounted to the translation carriage, is directly scanned along the surface under test at essentially constant distance between the AC and the SUT (Fig. 3). This allows application of the AC fixed-distance calibration, which, in our case, was done at the PTB [21] and transferred to the OSMS with a dedicated calibration system [63]. The payment for this advantage is a necessity to characterize and correct the wobbling error with an additional AC. The light beam aperture of the scanning AC is attached with a tube assembly, enclosing the AC optical path and suppressing air-convection noise [64]. To the best of our knowledge, the arrangement of an AC-based surface slope profilometer with a movable, vertically oriented AC and an additional AC in the reference channel was first considered in Ref. [65] and later implemented and published in Refs. [19-21,58].

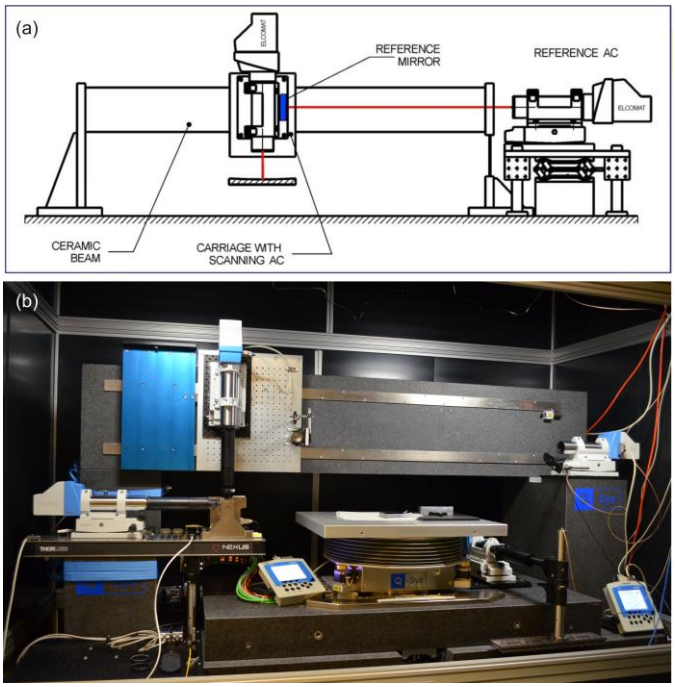

Figure 3. (a) Simplified schematic of the scanning gantry with a fixed distance autocollimator [60], and (b) as implemented on the ALS OSMS, with the aperture tube assembly attached to the AC [19-21]. The OSMS is capable of fully automatic two-dimensional surface slope mapping (see also paper [63] of the present conference).

The spatial resolution of the AC-based slope profilers is limited by the size of the light beam aperture [66]. Similar to the XROL OSMS arrangement in this paper, a circular aperture with a diameter of about 2.5 mm is typically used. A smaller aperture diameter leads to an increase of the profilometer's systematic error and loss of stability (repeatability) of the measurements [62]. Performance of the AC-based profilers with apertures of different shapes and sizes has been investigated in Ref. [21].

The accuracy of the ALS OSMS achieved in measurements with a significantly curved elliptical mirror with residual slope error of ~50 nrad (RMS) is on the level of 30 nrad (RMS) [66].

2.3 The ALS Developmental LTP

For completeness, we should mention one more surface slope profiler available at the ALS XROL. This is the Developmental LTP (DLTP) [52,53], a low-budget version of a NOM-like ELCOMAT-3000-based profiler. Originally created as a test-bed of new experimental methods, data acquisition techniques, and measurement control software, now the DLTP is routinely used for one-dimensional measurements with reflective optics in side-facing orientation [53]. Because of the similarity of the DLTP and OSMS AC sensors, here we do not separately measure and discuss the DLTP resolution.

Availability at the XROL of different metrology tools with similar functionality is crucial for increasing the confidence level of the metrology via cross-comparison of measurement performed with different tools with uncorrelated systematic errors.

3. ITF MEASUREMENTS WITH THE ALS LTP-II

For the ITF calibration of the slope profilers, we apply a method based on test surfaces with one-dimensional (1D) linear chirped height profiles of constant slope amplitude [23]. The two profiles of the chirped sample (the low and high frequency patterns) cover the spatial periods from ~ 1.1 mm to ~ 7.0 mm. Here, we present the ITF measurements performed over the low frequency pattern with range of periods of ~2.1–7.0 mm.

Fabrication of a chirped sample with variation of the height amplitude down to a few nanometers is a rather challenging task [67]. In order to verify the quality of the fabricated sample and determine the inherent slope distribution of the test patterns, the height profiles of the sample were accurately measured with a large field-of-view Fizeau interferometer and numerically differentiated to get the corresponding slope variations [21]. The obtained inherent slope variation amplitude of the chirped profiles is close to, but not exactly constant. Nevertheless, the fabricated sample allows precision ITF characterization of different slope profiles. For example, the high efficacy of the ITF calibration with the developed chirped sample has been recently validated in resolution characterization of the OSMS sample arm AC, equipped with apertures of different shapes and sizes [21].

3.1 The ITF of the ALS LTP-II in the SGB operation mode

In the SGB operation mode of the LTP-II, we use two algorithms for precisely positioning the detected light beam. One algorithm consists in fitting the intensity distributions, detected with the LTP-II CCD camera, with the Gaussian function and determining the position of its maximum. We call it the Gaussian maximum fitting (GMF) algorithm. Alternatively, the centroid of the intensity distributions is calculated. The later algorithm is called here the centroid-calculation positioning (CCP).

Figure 4 shows the slope profiles resulted in the two optional treatments of the intensity patterns. The measurement scan over the low-frequency pattern of the chirped sample was carried out with the LTP-II in the SGB operation mode.

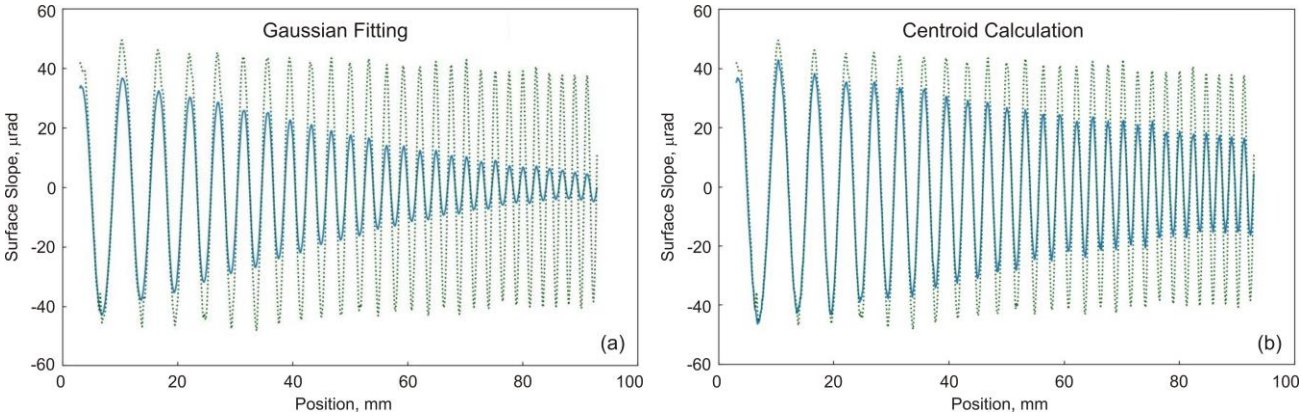

Figure 4. Slope profiles resulted in (a) the Gaussian maximum fitting and (b) centroid-calculation positioning of the intensity patterns recorded with the LTP-II in the SGB operation mode (the solid blue lines); (the dotted green lines) the inherent slope variation of the low-frequency pattern of the chirped sample as measured with a Fizeau interferometer with the effective pixel size of 0.1 mm.

The remarkable result in Fig. 4 is the significant difference, by a factor of ~ 4, of the slope variation amplitude at the highest spatial frequencies of about 0.5 mm,$^{-1}$ accessible with the low-frequency chirped profile. The surface slope evaluation based on the CCP algorithm provides the slope values much closer to the inherent slope data. Quantitatively, this observation can be characterized by the effective point spread functions of the LTP-II in the SGB operation mode with application of the Gaussian fitting or the centroid calculation, the SGB/GMF and the SGB/CCP operation modes, respectively.

On definition, the instrument's PSF describes its response to a point (delta-function-like) topographic object (see, for example, Refs. [10-12]). The effect of the PSF on the 1D surface slope measurements can be expressed as a convolution of the instrument's PSF with the inherent slope trace $\alpha_{INH}(x)$:

$$\alpha_{MES} = PSF * \alpha_{INH} \tag{1}$$

where α_{MES} is the measured trace and the symbol '*' denotes the convolution operation.

In the case of the LTP-II in the SGB operation mode, it is natural to use the PSF in the Gaussian form:

$$PSF = \left(2\pi\sigma^2\right)^{-1/2} \exp\left(-x^2/(2\sigma^2)\right), \tag{2}$$

where x is the position variable and σ^2 is the variance. For the measurements in Fig. 4, the values of the variance can be determined by best fitting the measured trace with the convolution expression (1).

The result of convolution of the inherent slope variation (as measured with the Fizeau interferometer) with the Gaussian PSF [Eq. (2)] with $\sigma = 0.463$ mm is depicted in Fig. 5a with the solid red line, together the trace, measured with the LTP-II in the SGB/CCP mode, shown in Fig. 5 with the dashed blue line.

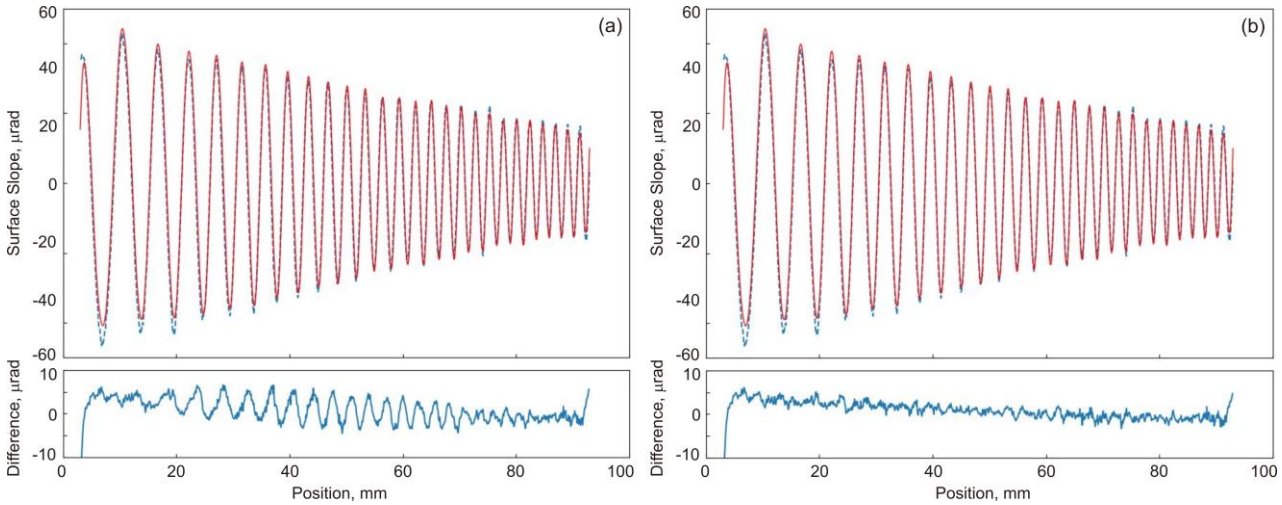

Figure 5. The slope profile measured with the LTP-II in the SGB/CCP mode (the dashed blue line) and (the solid red lines) the results of convolution of the Gaussian PSF [Eq. (2) with $\sigma = 0.463$ mm] and the inherent slope variation, (a) as measured with the Fizeau interferometer and (b) as additionally corrected for the interferometer geometric aberration. The bottom traces show the difference of the corresponding slope traces in the top plots; the RMS variations of the difference traces are (a) 2.78 µrad and (b) 2.13 µrad.

The RMS variation of the difference of the convolved and measured traces in Fig. 5a is 2.78 µrad, mainly due to the noticeable lateral mismatching of the traces over the central area of the sample. The mismatching appears in the difference as an oscillation with the amplitude varying approximately quadratically with the position along the sample. This can be due to the non-linearity of the LTP-II sampling or the geometric aberration of the interferometer. Having the LTP carriage translation precisely calibrated, we tested the former possibility with the simplest quadratic correction of the interferometric measurements.

Figure 5b presents the convolved inherent slope variation that was additionally corrected for the quadratic geometric aberration (the solid red line). Due to the correction, the oscillation in the difference trace is dissipated, and the RMS variation is decreased by ~30%.

Below in this paper, we will use as the inherent slope variation of the low-frequency chirped pattern the interferometric data corrected for the instrument's geometric aberration.

Figure 6 presents (the solid red lines) the results of modeling of the LTP-II PSF for the SGB/GMF operation mode (the dashed blue lines). Here, the Gaussian PSF [Eq. (2)] with $\sigma = 0.641\,\text{mm}$ is convolved with the inherent slope variation of the chirped sample. The corresponding PSD distributions are shown in Fig. 6b.

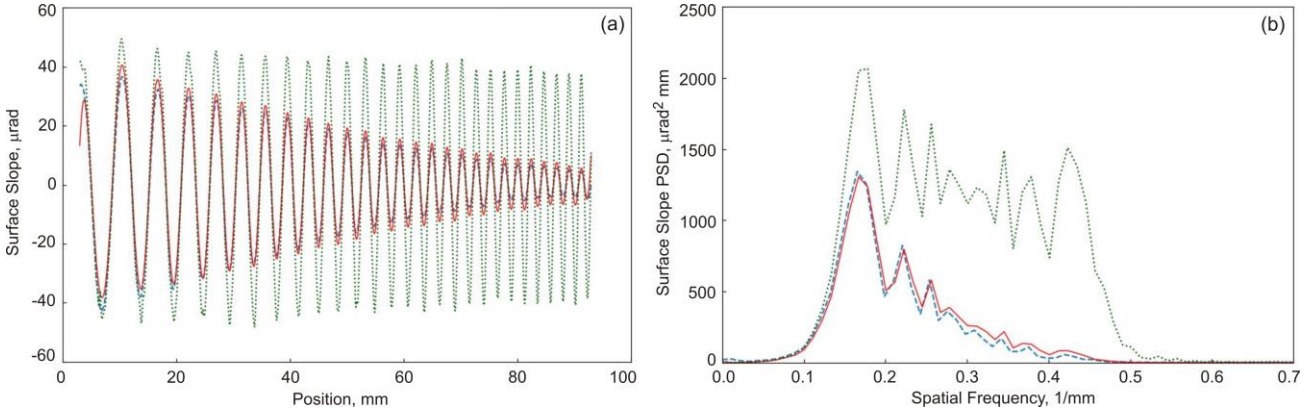

Figure 6. (a) The chirped sample slope profile as measured with the LTP-II in the SGB/GMF operation mode (the dashed blue line) and (the solid red lines) the results of convolution of the sample inherent slope variation (the dotted green line) with the Gaussian PSF [Eq. (2) with $\sigma = 0.641$ mm]; (b) the PSD distributions of the slope profiles in plot (a).

In the case of the LTP-II in the SGB/GMF mode (Fig. 6), the PSF in the form of Eq. (2) reasonably describes the drop of the measured amplitude. However, there is noticeable systematic overage of the convolved amplitude, increasing towards high spatial frequencies, that is clearly seen in the PSD distribution (Fig. 6b). This result, probably, can be explained by the deviation of the LTP-II beam intensity distribution (Fig. 7), measured in the LTP-II reference arm with a CCD camera placed before the reference mirror, from the Gaussian distribution.

There is one more problem in the data, obtained when measuring the resolution of the LTP-II, which requires an explanation. The values of the PSF variance, obtained in SGB/GMF and SGB/CCP operation modes, when converted to the effective values of the full-width-half-maximum (FWHM), lead to $FWHM_G \approx 1.51\,\text{mm}$ and $FWHM_C \approx 1.09\,\text{mm}$, respectively. These values are significantly larger than $FWHM_B \approx 0.853\,\text{mm}$ of the beam intensity distribution in Fig. 7.

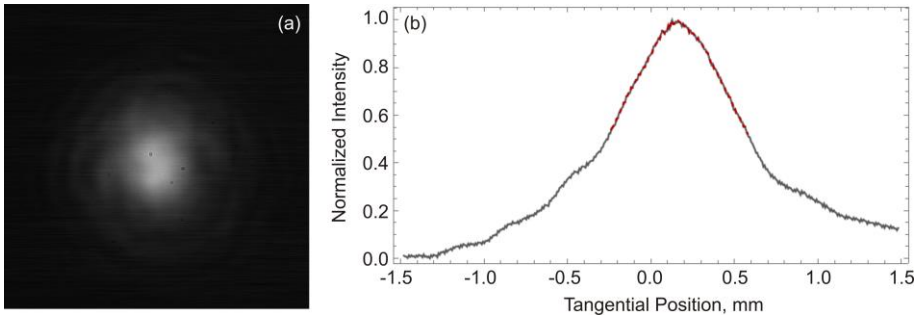

Figure 7. (a) Image of the reference-arm beam of the LTP-II in the SGB operation mode; (b) the one-dimensional intensity profile of the beam after integration of the 2D distribution in plot (a) in the sagittal direction. The value of the beam FWHM in the tangential direction is approximately 0.853 mm.

The difference of the measured FWHM of the LTP-II beam, $FWHM_B$, from the effective PSF values, $FWHM_G$ and $FWHM_C$, obtained by modeling of the LTP-II PSF in two different modes of data processing, is rather remarkable, especially for the case of the Gaussian fitting. It cannot be explained just by the deviation of the beam intensity distribution form the Gaussian shape, or by the difference of the beam sizes in the sample and reference arms.

We consider another explanation, related to the observed strong variation of the shape of the sample beam intensity distribution detected with the LTP-II CCD camera.

Video 1 shows the variation of the light beam intensity distributions in the reference arm (the left image) and (the right image) in the sample arm as detected with the LTP-II CCD camera. The data in the Video 1 corresponds to scanning the sensor of the LTP-II in the SGB operation mode along the chirped slope sample. The overall length of the trace presented in the video of ~ 65 mm corresponds to the higher spatial frequency part of the chirped pattern.

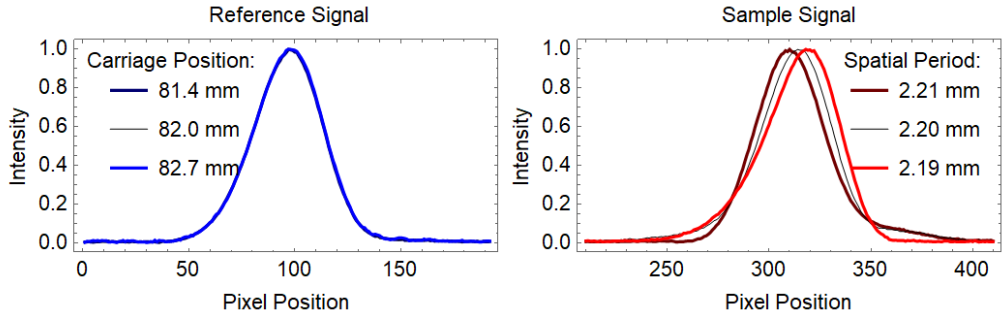

Video 1. The variation of the light beam intensity distributions in the reference arm (the left image) and (the right image) in the sample arm as recorded with the LTP-II in the SGB operation mode. The carriage position is changed with 0.1 mm increment. Besides the overall shift of the sample-arm intensity distribution, there is a strong variation of its shape. The shape change is due to the within-beam interference when different parts of the beam, reflected from the strongly aspheric SUT, have a difference in the optical path, and correspondingly, in the phase. http://dx.doi.org/doi.number.goes.here

In the course of the measurement, depicted in Video 1, the shape and the position of the intensity distribution recorded in the reference arm are almost unchanged. The small variation observed is mostly due to the carriage wobbling and light beam intensity instability. (Note that the LTP-II laser is tuned to stabilize frequency, rather than intensity.) This is unlike the behavior of the intensity distribution recorded in the sample arm, where besides the overall shift of the distribution, related to the sample slope variation, there is a strong variation of the distribution shape. The shape change is, probably, due to the within-beam interference when different parts of the beam, after reflection from the strongly aspheric SUT, such as the chirped pattern, have a difference in the optical path, and correspondingly, in the phase of some noticeable fraction of π (see also the data and discussion in Sec. 3.2).

When we find the beam position on the CCD detector with the GMF algorithm, we are ignoring the interference effect. This leads to the low resolution of the measurements with enlarged effective width of the PSF. On the contrary, the position of the intensity profile centroid accounts for the shape change and appears to be a better metric for the measurements, with higher resolution and the PSF with smaller width.

3.2 The ALS LTP-II in the PBI operation mode

In the PBI operation mode of the LTP-II, the two beams with the phase difference of approximately π are formed with the Porro prisms (Fig. 1a). The resultant light intensity distribution, measured with a CCD camera, placed in the reference arm, is shown in Fig. 8.

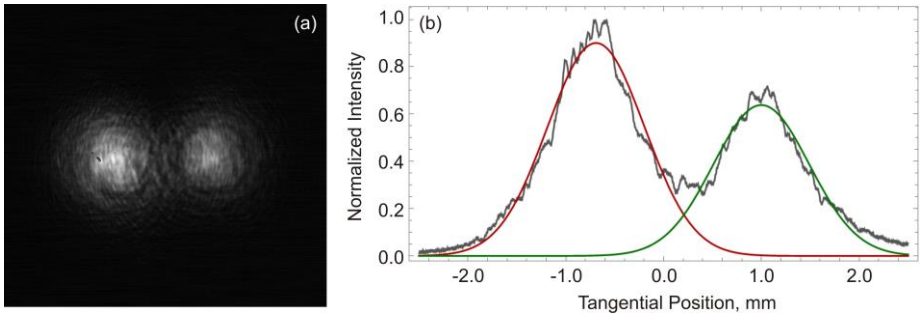

Figure 8. (a) Image of the reference-arm beam of the LTP-II in the PBI operation mode; (b) the one-dimensional intensity profile of the beam after integration of the 2D distribution in plot (a) in the sagittal direction. The value of the separation of the beams is approximately 1.8 mm. The smooth lines depict the result of fitting with two Gaussian distributions.

Due to the imperfections of the optics in the phase shifter, the intensity distribution is not perfectly symmetric. Fitting of the 1D profile in Fig. 8b with two shifted Gaussian functions provides the estimations for the beam separation of

~ 1.8 mm, the FWHM of ~ 0.70 mm (almost the same for the left and right beam), and the ratio of the beam intensities of ~ 0.71.

With the phase difference of approximately π, the intensity distribution in the focal plane of the FTL, recorded with the LTP-II detector, has a destructive character with the intensity minimum in the center.

Video 2 shows the variation of the light beam intensity distributions in the reference arm (the left image) and (the right image) in the sample arm as detected with the LTP-II CCD camera. In this case, the sensor of the LTP-II in the PBI operation mode is scanning along the chirped slope sample with 0.1 mm increment. The overall length of the trace, reproduced in Video 2, of ~ 65 mm corresponds to the higher spatial frequency part of the chirped pattern.

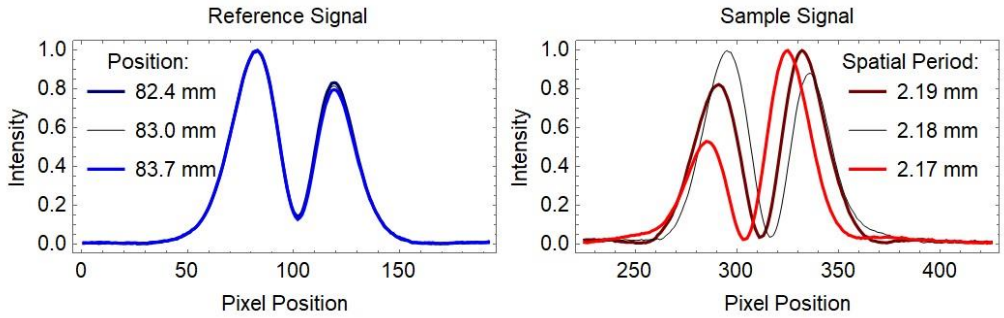

Video 2. The variation of the light beam intensity distributions in the reference arm (the left image) and (the right image) in the sample arm as recorded with the LTP-II in the PBI operation mode. Besides the overall shift of the two-peak fringe pattern in the sample-arm, there is a strong variation of its shape. The shape change is due to the interference of two components of the beam, which, after reflection from the strongly aspheric SUT, acquire an additional difference in the optical path, and correspondingly, in the phase. http://dx.doi.org/doi.number.goes.here

While the shape and the position of the two-peak destructive-interference-fringe pattern in the reference beam (the left-hand window in Video 2) are almost unchanged, the interference fringes recorded in the sample beam (the right-hand window in Video 2) have dramatic shape variation with the position along the chirped sample.

A similar change of the two-peak fringe pattern is routinely observed when the phase difference of the beam components is varied by the LTP-II phase shifter (Fig. 1a). This observation supports our hypothesis, stated in Sec. 3.1, about the origin of the shape variation of the detected intensity distribution due to the optical path difference, appearing in the beam reflected from a strongly aspheric SUT.

For precise determination of the measured slope angle from the detected intensity distribution in the LTP-II PBI operation mode, we use two algorithms.

The first algorithm realizes the classical PBI technique. In this case, position of the central minimum of the detected two-peak fringe pattern (Video 2) is determined by second-order-polynomial fitting (SOPF) of the central minimum in the pattern. The SOPF algorithm, which we use, is described and analyzed in detail in Ref. [13].

Similarly to the SGB operation mode, the second positioning algorithm, used in the PBI mode, is the CCP algorithm, which consists of calculation of centroid positions of the detected intensity distributions.

At first glance, for the case of the LTP-II in the PBI operation mode, it is natural to use the PSF in the form of two shifted Gaussian functions, describing the intensity distribution of two components of the sample and reference beams:

$$PSF_{2G} = A_{-}\exp\left(-(x-x_0)^2/(2\sigma_{-}^2)\right) + A_{+}\exp\left(-(x+x_0)^2/(2\sigma_{+}^2)\right), \quad (3)$$

where x_0 is the parameter of the beam-component position shift, A_{-} and A_{+} are the normalized intensities, and σ_{-}^2 and σ_{+}^2 are the variances of the beam components shifted in the negative and positive directions.

However, as we demonstrate below, a single Gaussian-function PSF [Eq. (2)] works well also to describe the resolution measurements with the LTP-II in the PBI/SOPF operation mode – Fig. 9.

Figure 9 presents the results of modeling of the LTP-II PSF for the case of the PBI/SOPF operation mode. The solid red line depicts the result of convolution of the single Gaussian function PSF [Eq. (2)] with $\sigma = 0.772$ mm with the inherent slope variation of the chirped sample (the dotted green line). The corresponding PSD distributions are shown in Fig. 9b.

There is a remarkable matching of the convolution results and the measured data (the dashed blue lines in Fig. 9). Therefore, the single Gaussian function proves to be an adequate model for the PSF of the LTP-II in the classical PBI/SOPF arrangement. However, in this case, the resolution appears to be lower by a factor of ~ 1.67 than that of the SGB/CCP mode (compare with the data in Fig. 5).

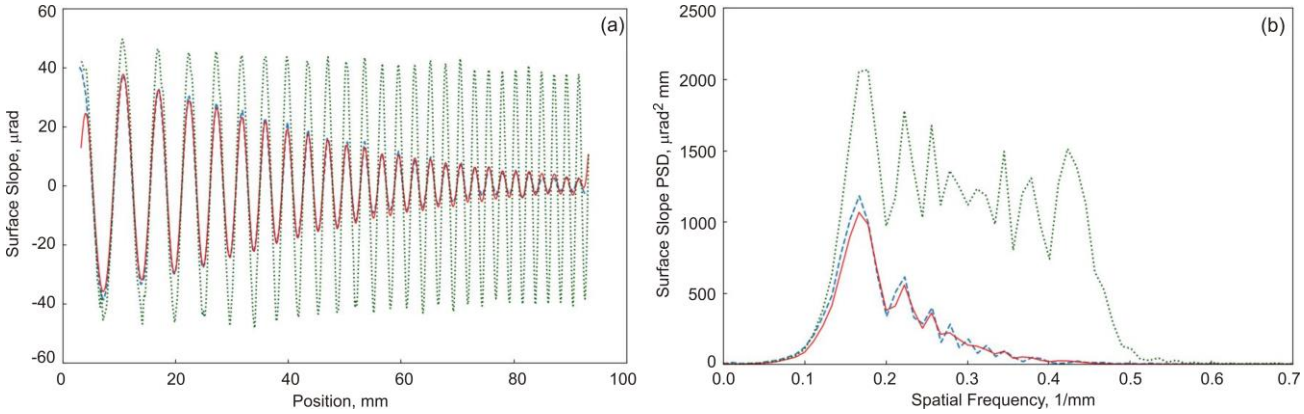

Figure 9. (a) The chirped sample slope profile measured with the LTP-II in the PBI/SOPF mode (the dashed blue line), and (the solid red line) the results of convolution of the sample inherent slope variation (the dotted green line) with the Gaussian PSF [Eq. (2)] with $\sigma = 0.772$ mm; (b) the PSD distributions of the profiles in plot (a).

Results of the resolution measurements with the LTP-II in the PBI/CCP operation mode are depicted in Fig. 10. In this case, the profiler's PSF can be precisely modeled with the two-Gaussian function, given with Eq. (3).

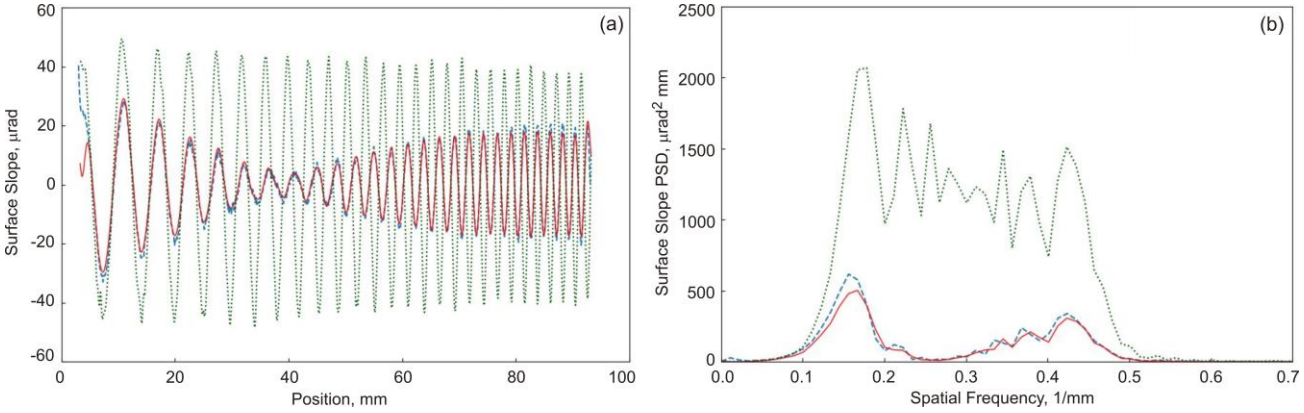

Figure 10. (a) The chirp sample slope profile, measured with the LTP-II in the PBI/CCP operation mode (the dashed blue line), and (the solid red line) the results of convolution of the sample inherent slope variation (the dotted green line) with the two-Gaussian PSF [Eq. (3)] with $x_0 = 0.958$ mm, $\sigma_- = \sigma_+ = 0.416$ mm, and $A_-/A_+ = 0.81$; (b) the PSD distributions of the profiles in plot (a).

An important new feature of the data in Fig. 10 is a flip of the sign of the measured slope variation at the position of ~ 40 mm that corresponds to the spatial period of the chirped sample of ~ 3.5 mm. The flip is the known signature of an ITF with negative periods (see, for example Refs. [10-12]).

Because the Fourier transform of a Gaussian function is also Gaussian function, the ITF, corresponding to the PSF, defined with Eq. (2), has not negative periods and, therefore, the single Gaussian function is not suitable for modeling the PSF of the LTP-II in PBI operation mode with centroid-calculation positioning.

In order to model the PSF of the LTP-II in this arrangement, we use the two-Gaussian function, given with Eq. (3). With the parameters of the model: $x_0 = 0.958$ mm, $\sigma_- = \sigma_+ = 0.416$ mm, and $A_-/A_+ = 0.81$ (the later ratio accounts for the asymmetrical shape of the beam intensity distribution in Fig. 8), we get the PSF, sketched in Fig. 11 together with the corresponding ITF.

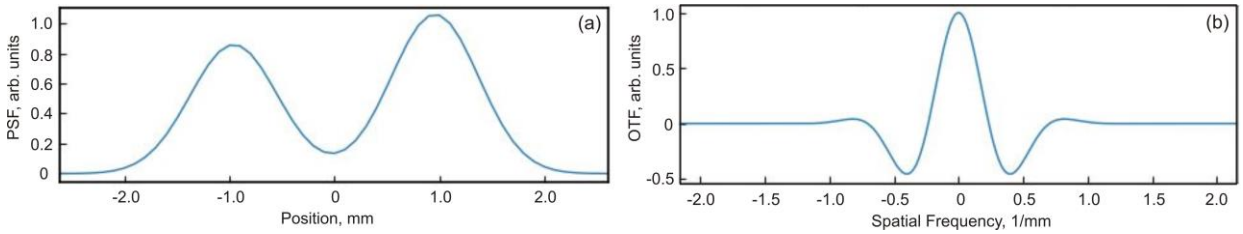

Figure 11. (a) The PSF and (b) the ITF of the LTP-II in the PBI/CCP operation mode with the centroid-calculation positioning of the recorded two-peak intensity patterns.

The PSF in Fig. 11a convolves the chirped-sample inherent slope distribution to closely match the measured trace (the dashed blue line in Fig. 10a). The close matching of the corresponding PSD spectra in Fig. 10b also supports the validity of the approximation of the PSF with the two-Gaussian model in Eq. (3).

4. THE LTP-II RESOLUTION IN COMPARISON WITH THE OSMS

In Sec. 4.1, below, we discuss the resolution of the ALS OSMS with 2.5-mm-diameter aperture that is the classical arrangement of a slope profiler based on autocollimator ELCOMAT-3000. The spatial resolution of the OSMS equipped with apertures of different size and shapes has been comprehensively investigated in the recent publication [21].

In Secs. 4.2 and 4.3, the resolution of the OSMS is compared with that of the ALS LTP-II in two operation modes, SGB/CCP and PBI/CCP. These modes provide larger amplitudes of the slope variation at higher spatial frequencies of the chirped pattern, measured with the LTP-II in the SGB and PBI arrangements, respectively (see Sec. 3).

4.1 Spatial resolution of the ALS OSMS equipped with a circular aperture of 2.5-mm diameter

Figure 12 shows (the dashed blue lines) the results of resolution measurements with the ALS OSMS equipped with a circular aperture of 2.5-mm diameter. The measurements were performed over the same low-spatial-frequency pattern of the chirped slope sample. Note that the data in Fig. 12 are also relevant to the classical arrangement of a NOM-like slope profiler with an autocollimator ELCOMAT-3000-based sensor with a circular aperture of 2.5-mm diameter [46-58].

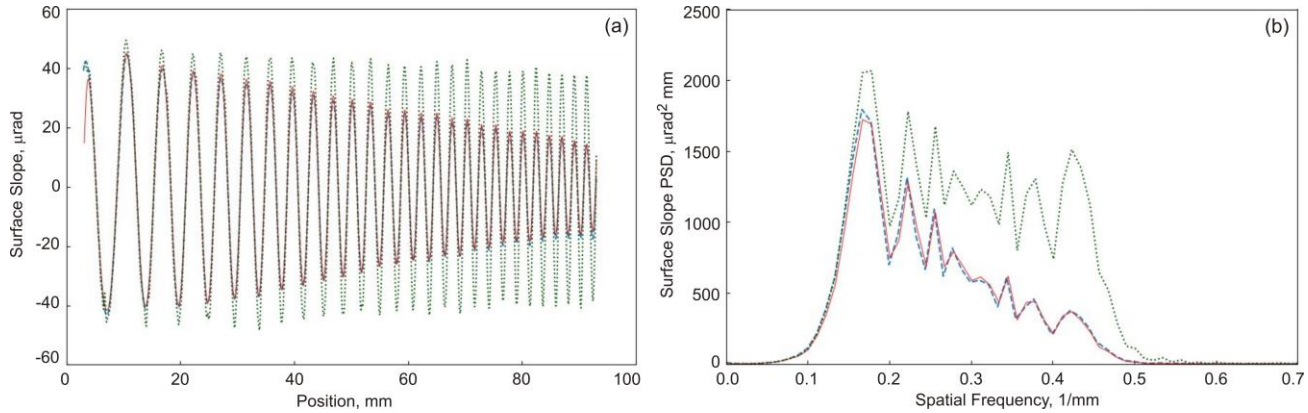

Figure 12. (a) The chirped-sample slope profile (the dashed blue line), as measured with the ALS OSMS equipped with a circular aperture of 2.5-mm diameter, and (the solid red line) the result of convolution of the sample inherent slope variation with the 'NOM-approximation' ITF, derived in Ref. [66]. For reference, the inherent slope variation of the chirped pattern is shown with the dotted green line; (b) the PSD distributions of the profiles in plot (a).

The resolution properties of the OSMS with 2.5-mm aperture are well described with a circular aperture ITF, analytically derived in [68] and corrected in Ref. [66] with an additional term, empirically determined to better match the OSMS resolution measurements with the high-spatial-frequency pattern of the chirped slope test sample [22,23], used also here:

$$ITF_{NOM} = \frac{J_1(2\pi a u)}{\pi a u}\left(1 + C \cdot u^3\right), \tag{4}$$

which we call 'NOM approximation' ITF.

In Eq. (4), J_1 is the first order Bessel function of the first kind, u is the frequency variable, and $a \approx 0.73$ mm is the effective radius of the aperture; the optimized value of the parameter C is $C \approx 3.7 \cdot 10^{-6}$ [66]. Note that the effective diameter of $2a \approx 1.46$ mm of the 'NOM approximation' ITF [Eq. (4)] is significantly smaller than the AC aperture diameter of 2.5 mm. This is probably due to the rather complicated algorithm, used in the AC ELCOMAT-3000 to evaluate the measured angle [69].

In Fig. 12a, the slope trace, shown with the solid red line, is obtained by application of the ITF, given with Eq. (4), to the inherent slope distribution of the low-frequency pattern of the chirped sample (the dotted green line in Fig. 12a). This processed trace almost perfectly coincides with the measured slope distribution (the dashed blue line in Fig. 12a). The corresponding PSD distributions, shown in Fig. 12b, illustrate in the spatial frequency domain the high confidence of the OSMS ITF model, given with Eq. (4).

4.2 LTP-II in the SGB/CCP operation mode vs OSMS

For better comparison of the lateral resolution of the LTP-II in the SGB/CCP operation mode and the OSMS with 2.5-mm aperture, in Fig. 13 we put together the results of the resolution measurements for these two slope profilers, discussed in detail in Secs. 3.1 and 4.1, respectively.

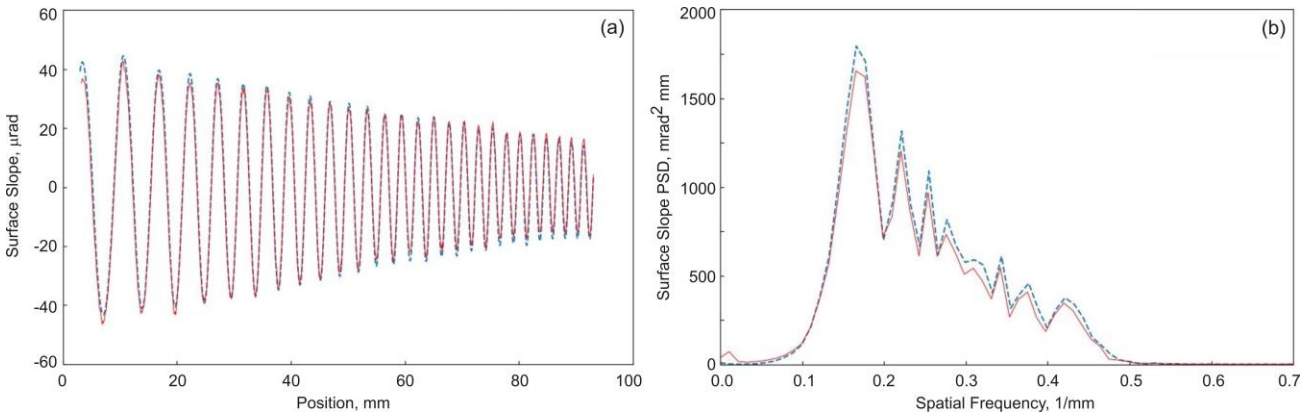

Figure 13. (a) The slope profiles and (b) the corresponding PSD distributions of the low-frequency pattern of the chirped sample as measured (the solid red line) with the LTP-II in the SGB/CCP mode of operation, and (the dashed blue line) with the OSMS equipped with a circular aperture of 2.5-mm diameter.

Over the spatial wavelength range of ~ 2.1–7.0 mm, covered with the low-frequency pattern of the chirped sample, the lateral resolution of the LTP-II in the SGB/CCP mode of operation, and the OSMS with 2.5-mm-diameter aperture is the same. Therefore, from the point of view of resolution, the tools are equivalent.

The lateral resolution of an AC ELCOMAT-3000 based slope profiler can be improved by a factor of ~ 1.5 with the use of a rectangular aperture of 1.5 mm x 3 mm, as first suggested and demonstrated in Ref. [21]. As to the LTP-II in the SGB mode, the resolution boundary is set by the diffraction-limited light-beam-spot size probing the SUT. The decrease of the spot size with an additional focusing lens, as suggested, for example, in Ref. [70], does not seem to be a good practical solution because of the additional problems, such as the uncertainty in the angular calibration of such a profiler.

4.3 LTP-II in the PBI/CCP operation mode vs OSMS

On the contrary to the LTP-II in the SGB/CCP mode, the resolution properties of the LTP-II in the PBI/CCP operation mode is significantly different from that of the OSMS – Fig. 14.

Over the lower-frequency part of the chirped pattern, the PBI/CCP LTP-II measurements (the solid green lines in Fig. 14) provide the slope variation amplitude smaller than the OSMS by a factor of > 2. The measured amplitude falls to zero at the spatial wavelength of ~ 3.5 mm and flips the phase of the variation over the higher-frequency part of the

pattern. An interesting observation in Fig. 14 is at the wavelength of ~ 2.3 mm, where the slope variation amplitude, measured with the LTP-II in the PBI/CCP mode overreaches that measured with the OSMS with 2.5-mm aperture.

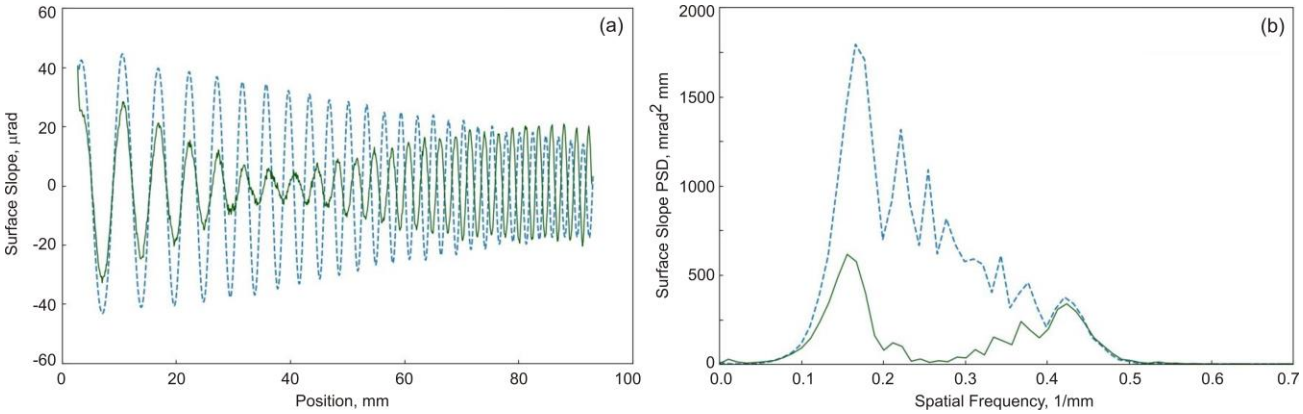

Figure 14. (a) The slope profiles and (b) the corresponding PSD distributions of the low-frequency pattern of the chirped sample as measured with the LTP-II in the PBI/CCP operation mode (the solid green lines) and (the dashed blue lines) with the OSMS equipped with a circular aperture of 2.5-mm diameter.

Therefore, if ignoring the wrong phase of the variation amplitude, the LTP-II in the PBI/CCP mode provides data that are more reliable only over a rather narrow spatial wavelength range of ~ 2 – 2.5 mm.

At first glance, this observation leads to the conclusion that the LTP-type tools cannot compete with the AC ELCOMAT-3000-based slope profilers. However, this is not the case.

There are a few significant advantages provided by the LTP-type slope profilers. First, when equipped with a single-mode laser light source, the LTP allows precision characterization of groove-density distribution of diffraction gratings [34,41,42]. This is impossible with the ELCOMAT-3000 that uses a broad-band non-coherent LED light source. Second, unlike the AC-based tools, the LTP profilers do not require a light limiting aperture. This simplifies measurements with optical assemblies. Third, specifically for the ALS LTP-II gantry system, it has a capability for lifting the LTP sensor to increase the clearance needed for measurements with large multi-component optical assemblies. Finally, there is still an open question about the possibility to control/monitor the LTP systematic errors when using the LTP in different operation modes, as first discussed in Ref. [16].

5. APPLICATION OF THE MEASURED ITF

For the completeness of the discussion in this paper, centered to the resolution measurements with the LTP-II in different operation modes, we present below a few examples of application of the knowledge about the instrument's PSF and ITF (obtained via the dedicated measurements and modeling, as discussed in Secs. 3 and 4) to improve the quality (reliability) of the metrology data.

A detailed discussion of the involved analytical methods and dedicated numerical techniques and software is out of the scope of the present work. Some introductory information can be found in Ref. [68]. In this publication, the ITF-based reconstruction (deconvolution) of the measured slope data beyond the instrumental resolution limit was first suggested and demonstrated on the example of a 1D data, forecasted using stochastic modeling of the measured data. A comprehensive description of the reconstruction methods and newly dedicated software are presented in a recent work [66]. It also discusses the results of application of the developed methods and software to sophisticated treatment of 1D surface slope data, obtained with the ALS XROL OSMS.

Figures 15 and 16 illustrate the efficiency of resolution-measurement-based reconstruction of the chirped sample slope variation from the slope traces measured with the LTP-II in the SGB/CCP and PBI/CCP modes of operation. For comparison, similar data from the chirped-sample slope metrology with the OSMS with 2.5-mm-diameter aperture is shown in Fig. 17.

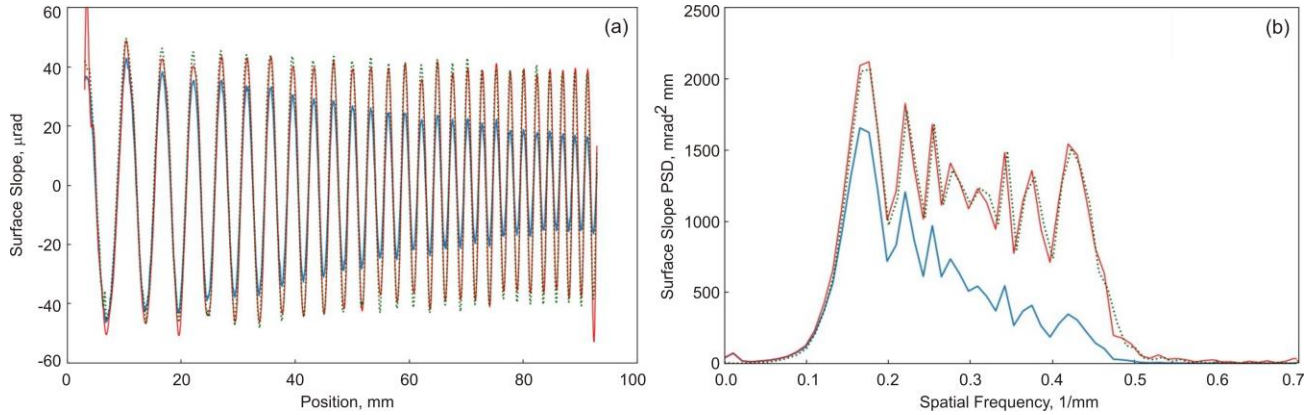

Figure 15. (a) The slope profiles and (b) the corresponding PSD distributions of the low-frequency pattern of the chirped sample as measured (the blue dashed lines) with the LTP-II in the SGB/CCP mode of operation, and (the solid red lines) as obtained in the course of reconstruction process, developed in Ref. [66]. For reference, the inherent slope variation and its PSD of the chirped pattern are shown with the dotted green lines.

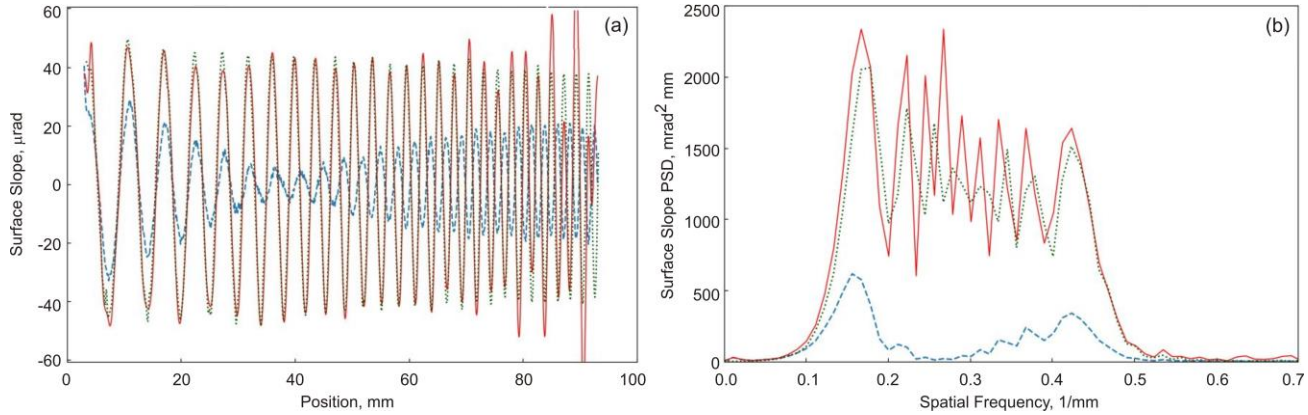

Figure 16. (a) The slope profiles and (b) the corresponding PSD distributions of the low-frequency pattern of the chirped sample as measured (the blue dashed lines) with the LTP-II in the PBI/CCP mode of operation, and (the solid red lines) as obtained in the course of reconstruction process, developed in Ref. [66]. For reference, the inherent slope variation and its PSD of the chirped pattern are shown with the dotted green lines.

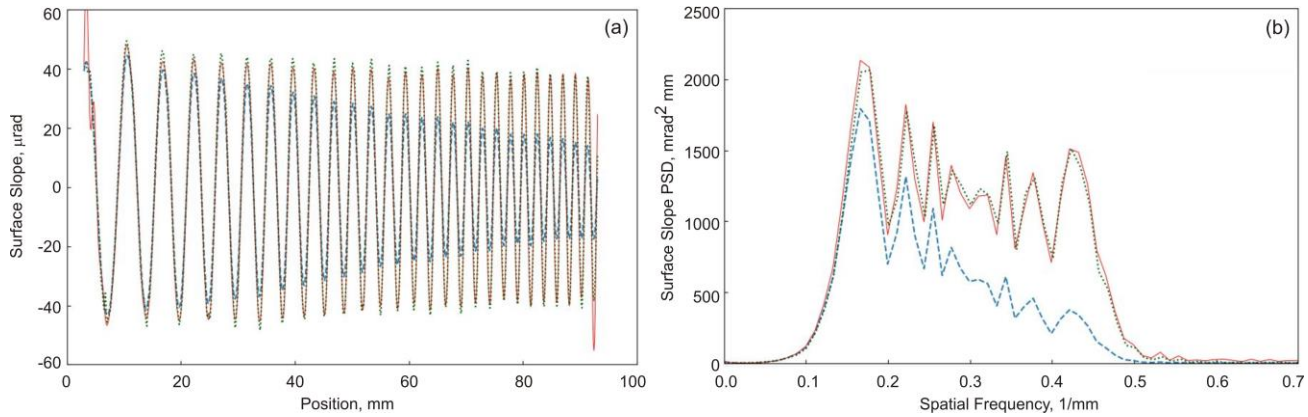

Figure 17. (a) The slope profiles and (b) the corresponding PSD distributions of the low-frequency pattern of the chirped sample as measured (the blue dashed lines) with the OSMS with 2.5-mm-diameter circular aperture, and (the solid red lines) as obtained in the course of reconstruction process, developed in Ref. [66]. For reference, the inherent slope variation and its PSD of the chirped pattern are shown with the dotted green lines.

In all three cases in Figs. 15 – 17, the reconstruction process, developed in Ref. [66], allows to effectively improve the resolution of the measurements and provides the recovered (processed) slope traces that almost exactly match the inherent slope distribution of the chirped profile under measurements.

However, with the data, measured with the LTP-II in the PBI/CCP operation mode (Fig. 16), the reconstruction gives slightly worse result. This is because the PBI/CCP LTP-II measurement suffers from the loss of information around the point of the ITF zero crossing.

The two other options of slope profilometry, the LTP-II in the SGB/CCP mode of operation (Fig. 15) and the OSMS with 2.5-mm-diameter circular aperture, have the single-Gaussian-like ITFs without zero crossings. Therefore, their measurements contain complete information about the sample surface profile over the entire spatial frequency range, characteristic for the sample. This information together with the knowledge about the ITFs of the instruments are sufficient for obtaining upon reconstruction the high confidence slope metrology of the chirped sample.

6. DISCUSSION AND CONCLUSIONS

We have presented the results of a comprehensive investigation of spatial (lateral) resolution of the LTP-II and OSMS surface slope profilers, both available at the ALS X-Ray Optics Laboratory. These are the tools of the surface slope profilometry types, most commonly used for high accuracy characterization of x-ray optics in the low-spatial-frequency range.

We have shown that, when the LTP-II is used in the single Gaussian beam arrangement and the positioning of the intensity distribution of the detected light beam is performed by calculation the distribution centroid (the LTP-II in the SGB/CCP mode), its ITF can be accurately modeled with a single Gaussian function. Comparison of the SGB/CCP LTP-II resolution with that of the OSMS, equipped with 2.5-mm-diameter aperture, depicts almost identical resolution properties over the spatial frequency range, covered with the chirped slope pattern of the sample used in this work for the ITF calibration.

We have experimentally demonstrated that the LTP in the SGB mode with positioning based on fitting the detected intensity distribution with the Gaussian function (the LTP-II in the SGB/GMF mode) has significantly lower resolution.

Our investigation on resolution of the LTP-II in a classical two-beam pencil-beam-interferometer arrangement have established that the classical positioning algorithm, based on determining the position of the minimum of the detected destructive-interference-fringe pattern (the LTP-II in the PBI/SOPF mode), significantly reduces, by a factor of ~ 1.67, the resolution compared with the LTP-II in the SGB/CCP mode and the OSMS with a 2.5-mm aperture. Note that, the single Gaussian function has been shown to be an adequate model for the PSF of the LTP-II in the classical PBI/SOPF arrangement.

The LTP-II in the PBI arrangement with the centroid calculation positioning (the LTP-II in the PBI/CCP mode), can still compete in the resolution with other two profilometry options (the LTP-II in the SGB/CCP mode and the OSMS with a 2.5-mm aperture). If ignoring the wrong phase of the variation amplitude, the LTP-II in the PBI/CCP mode provides data that are more reliable over spatial wavelength range of ~ 2 – 2.5 mm. In order to model the PSF of the LTP-II in the PBI/CCP mode, we have suggested to use the two-Gaussian function. With the properly optimized parameters, the PSF allows us to precisely describe the experimental data, obtained with the chirped slope sample.

We have also discussed the application of the knowledge about the instrument's PSF and ITF (obtained via the dedicated measurements and modeling, as shown in this paper) to improve the quality (reliability) of 1D slope metrology data. Without a detailed discussion of the involved analytical methods and dedicated numerical techniques and software (that can be found in Refs. [66,68]), we have demonstrated the possibility of resolution-measurement-based reconstruction of the chirped sample slope variation from the slope traces measured with the LTP-II in the SGB/CCP and PBI/CCP modes of operation, and with the OSMS with a 2.5-mm aperture. In all three cases, the reconstruction allows to effectively improve the resolution of the measurements and provides the recovered (processed) slope traces that almost exactly match the inherent slope distribution of the chirped profile under measurements.

At first glance, our investigation leads to the conclusion that the LTP-type tools cannot compete with the AC ELCOMAT-3000-based slope profilers. However, this is not the case.

There are a few significant advantages provided by the LTP-type slope profilers. First, when equipped with a single-mode laser light source, the LTP allows precision characterization of groove-density distribution of diffraction gratings

[34,41,42]. This is impossible with the ELCOMAT-3000 that uses a broad-band non-coherent LED light source. Second, unlike the AC-based tools, the LTP profilers do not require a light limiting aperture, placed close to the SUT. This simplifies measurements with optical assemblies. Third, specifically for the ALS LTP-II gantry system, it has a capability for lifting the LTP sensor to increase the space, needed for measurements with large multi-component optical assemblies. Finally, there is still open the question about the possibility to control/monitor the LTP systematic errors when using the LTP in different operation modes, as first discussed in Ref. [16].

The work on numerical simulation of the experimental results of this paper, using a comprehensive optical modeling of the LTP-II, is in progress and will be discussed elsewhere.

ACKNOWLEDGEMENTS

This work was performed in the scope of the subcontract with Rochester Scientific, LLC, supported by the U.S. Department of Energy STTR program on industrialization of the BPRA based MTF calibration technique under Award Numbers DE-SC0011352 to aBeam Technologies, Inc. Research at the Advanced Light Source at Lawrence Berkeley National Laboratory are DOE Office of Science User Facilities under contract no. DE-AC02-05CH11231.

DISCLAIMER

REFERENCES

[1] ALS-U, https://als.lbl.gov/als-u/.

[2] Kevan, S., Chair, [ALS-U: Solving Scientific Challenges with Coherent Soft X-Rays], Workshop report on early science enabled by the Advanced Light Source Upgrade, ALS, LBNL, Berkeley, CA, (2017) https://als.lbl.gov/wp-content/uploads/2017/08/ALS-U-Early-Science-Workshop-Report-Full.pdf.

[3] Samoylova, L., Sinn, H., Siewert, F., Mimura, H., Yamauchi, K., and Tschentscher, T., "Requirements on hard X-ray grazing incidence optics for European XFEL: Analysis and simulation of wavefront transformations," Proc. SPIE 7360, 73600E/1-9 (2009). <https://doi.org/10.1117/12.822251>.

[4] Cocco, D., "Recent Developments in UV optics for ultra-short, ultra-intense coherent light sources," Photonics 2015, 2(1), 40-49 (2015). <https://doi.org/10.3390/photonics2010040>.

[5] Yashchuk, V. V., Samoylova, L., and Kozhevnikov, I. V., "Specification of x-ray mirrors in terms of system performance: new twist to an old plot," Opt. Eng., 54(2), 025108 (2015). <https://doi.org/10.1117/1.OE.54.2.025108>.

[6] Yashchuk, V. V., Samoylova, L., and Kozhevnikov, I. V., "Specification of x-ray mirrors in terms of system performance: A new twist to an old plot," Proc. SPIE 9209, 92090F/1-19 (2014). <https://doi.org/10.1117/12.2062085>.

[7] Siewert, F., Buchheim, J., Gwalt, G., Bean, R., and Mancuso, A. P., "On the characterization of a 1 m long, ultra-precise KB-focusing mirror pair for European XFEl by means of slope measuring deflectometry," Rev. Sci. Instrum. 90, 021713 (2019). <https://doi.org/10.1063/1.5065473>.

[8] Yashchuk, V. V., Artemiev, N. A., Lacey, I., McKinney, W. R., and Padmore, H. A., "Advanced environmental control as a key component in the development of ultra-high accuracy ex situ metrology for x-ray optics," Opt. Eng. 54(10), 104104/1-14 (2015). <https://doi.org/10.1117/1.OE.54.10.104104>.

[9] Yashchuk, V. V., Artemiev, N. A., Lacey, I., McKinney, W. R., and Padmore, H. A., "A new X-ray optics laboratory (XROL) at the ALS: Mission, arrangement, metrology capabilities, performance, and future plans," Proc. SPIE 9206, 92060I/1-19 (2014). <https://doi.org/10.1117/12.2062042>.
[10] Boreman, G. D., [Modulation Transfer Function in Optical and Electro-optical Systems], SPIE Press, Bellingham, Washington (2001).
[11] Kay, S. M., [Modern Spectral Estimation: Theory and Application], Prentice Hall, Englewood Cliffs (1988).
[12] Jenkins, G. M. and Watts, D. G., [Spectral Analysis and its Applications], Fifth Printing: Emerson-Adams Press, Boca Raton (2007).
[13] Yashchuk, V. V., "Positioning errors of pencil-beam interferometers for long-trace profilers," Proc. SPIE 6317, 63170A/1-12 (2006). <https://doi.org/10.1117/12.677956 >.
[14] Kirschman, J. L., Domning, E. E., McKinney, W. R., Morrison, G. Y., Smith, B. V., and Yashchuk, V. V., "Performance of the upgraded LTP-II at the ALS Optical Metrology Laboratory," Proc. SPIE 7077, 70770A/1-12 (2008). <https://doi.org/10.1117/12.796335>.
[15] Ali, Z., Artemiev, N. A., Cummings, C. L., Domning, E. E., Kelez, N., McKinney, W. R., Merthe, D. J., Morrison, G. Y., Smith, B. V., and Yashchuk, V. V., "Automated suppression of errors in LTP-II slope measurements with x-ray optics," Proc. SPIE 8141, 81410O-1-15 (2011). <https://doi.org/10.1117/12.894061>.
[16] Centers, G., Smith, B. V., and Yashchuk, V. V., "New operational mode of the pencil beam interferometry based LTP," Proc. SPIE 9962, 996202/1-13 (2016). < https://doi.org/10.1117/12.2238298>.
[17] Nikitin, S. M., Gevorkyan, G. S., McKinney, W. R., Lacey, I., Takacs, P. Z., and Yashchuk, V. V., "New twist in the optical schematic of surface slope measuring long trace profiler," Proc. SPIE 10388, 103850I-1-17 (2017). <https://doi.org/10.1117/12.2274400>.
[18] Lacey, I., Adam, J., Centers, G., Gevorkyan, G. S., Nikitin, S. M., Smith, B. V., and Yashchuk, V. V., "Development of a high performance surface slope measuring system for two-dimensional mapping of x-ray optics," Proc. SPIE 10385, 103850G (2017). <https://doi.org/10.1117/12.2273029>.
[19] Lacey, I., Anderson, K., Centers, G. P., Geckeler, R. D. Gevorkyan, G. S., Just, A., Nicolot, T., Smith, B. V., and Yashchuk, V. V., "The ALS OSMS: Optical Surface Measuring System for high accuracy two-dimensional slope metrology with state-of-the-art x-ray mirrors," Proc. SPIE 10760, 1076002 (2018). <https://doi.org/10.1117/12.2321347>.
[20] Yashchuk, V. V., Centers, G., Gevorkyan, G. S., Lacey, I., and Smith, B. V., "Correlation methods in optical metrology with state-of-the-art x-ray mirrors," Proc. SPIE 10612, 106120O (2018). <https://doi.org/10.1117/12.2305441>.
[21] Lacey, I., Geckeler, R. D., Just, A., Siewert, F., Arnold, T., Paetzelt, H., Smith, B. V., and Yashchuk, V. V., "Optimization of size and shape of aperture in autocollimator-based deflectometric profilometers," Rev. Sci. Instrum. 90(2), 021717 (2019). <https://doi.org/10.1063/1.505871>.
[22] Siewert, F., Buchheim, J., Höft, T., Zeschke, T., Schindler, A., and Arnold, T., "Investigations on the spatial resolution of autocollimator-based slope measuring profilers," Nucl. Instrum. Methods A 710, 42–47 (2013). <https://doi.org/10.1016/j.nima.2012.10.130>.
[23] Siewert, F., Zeschke, T., Arnold, T., Paetzeld, H., and Yashchuk, V. V., "Linear chirped slope profile for spatial calibration in slope measuring deflectometry," Rev. Sci. Instrum. 87(5), 051907/1-8 (2016). <https://doi.org/10.1063/1.4950737>.
[24] von Bieren, K., "Pencil Beam Interferometer For Aspherical Optical Surfaces," Proc. SPIE 343, 101 (1982). <https://doi.org/10.1117/12.933743>.
[25] von Bieren, K., "Interferometry of wave fronts reflected off conical surfaces," Appl. Opt. 22, 2109-2114 (1983). <https://doi.org/10.1364/AO.22.002109>.
[26] von Bieren, K., "Pencil beam interferometer," US Patent 4,498,773 (1985).
[27] Takacs, P. Z., Qian, S., and Colbert, J., "Design of a long trace surface profiler," Proc. SPIE 749, 59-64 (1987). <https://doi.org/10.1117/12.939842>.
[28] Takacs, P. Z., Feng, S. K., Church, E. L., Qian, S., and Liu, W-M., "Long trace profile measurements on cylindrical aspheres," Proc. SPIE 966, 354-64 (1989). <https://doi.org/10.1117/12.948082>.
[29] Irick, S. C., McKinney, W. R., Lunt, D. L. T., and Takacs, P. Z., "Using a straightness reference in obtaining more accurate surface profiles," Rev. Sci. Instrum. 63, 1436–1438 (1992). <https://doi.org/10.1063/1.1143036>.
[30] Irick, S. C., "Improved measurement accuracy in a long trace profiler: compensation for laser pointing instability," Nucl. Instrum. Methods Phys. Res. A 347, 226–230 (1994). <https://doi.org/10.1016/0168-9002(94)91882-1>.

[31] Li, H., Takacs, P. Z., and Oversluizen, T., "Vertical scanning long trace profiler: a tool for metrology of x-ray mirrors," Proc. SPIE 3152,180–187 (1997). <https://doi.org/10.1117/12.295557>.
[32] Takacs, P. Z., Church, E. L., Bresloff, C. J., Assoufid, L., "Improvements in the accuracy and the repeatability of long trace profiler measurements," Appl. Optics 38(25), 5468-5479 (1999). <https://doi.org/10.1364/AO.38.005468>.
[33] Qian, S. N., Takacs, P., Sostero, G., and Cocco, D., "Portable long trace profiler: Concept and solution," Rev. Sci. Instrum. 72(8), 3138-3204 (2003). <https://doi.org/10.1063/1.1384452>.
[34] Cocco, D., Sostero, G., and Zangrando, M., "Technique for measuring the groove density of diffraction gratings using the long trace profiler," Rev. Sci. Instrum. 74(7), 3544-3548 (2003). <https://doi.org/10.1063/1.1584080>.
[35] Rommeveaux, A., Hignette, O., and Morawe, C., "Mirror metrology and bender characterization at ESRF," Proc. SPIE 5921, 59210N/1-8 (2005). <https://doi.org/10.1117/12.621379>.
[36] Rommeveaux, A., Thomasset, M., and Cocco, D., "The Long Trace Profilers," in [Modern Developments in X-ray and Neutron Optics], A. Erko, M. Idir, T. Krist, A. G. Michette, Eds., Chapter 10, Springer-Verlag, Berlin/Heidelberg (2008).
[37] Thomasset M. and Polack, F., "Characterization of optical surfaces for the present generations of synchrotron sources," Proc. SPIE 7155, 715506/1-12 (2008). <https://doi.org/10.1117/12.814695>.
[38] Senba, Y., Kishimoto, H., Ohashi, H., Yumoto, H., Zeschke, T., Siewert, F., Goto, S., Ishikawa, T., "Upgrade of long trace profiler for characterization of high-precision X-ray mirrors at SPring-8," Nucl. Instrum. and Methods A 616(2-3), 237-240 (2010). <https://doi.org/1010.1016/j.nima.2009.12.007>.
[39] Qian, J., Sullivan, J., Erdmann, M., and Assoufid, L., "Performance of the APS optical slope measuring system," Nucl. Instr. and Meth. A 710, 48-51 (2013). <https://doi.org/10.1016/j.nima.2012.10.102>.
[40] Yashchuk, V. V., Artemiev, N. A., Centers, G., Chaubard, A., Geckeler, R. D., Lacey, I., Marth, H., McKinney, W. R., Noll, T., Siewert, F., Winter, M., and Zeschke, T., "High precision tilt stage as a key element to universal test mirror for characterization and calibration of slope measuring instruments," Rev. Sci. Instrum. 87(5), 051904 (2016). <https://doi.org/10.1063/1.4950729>.
[41] Thomasset, M., Dvorak, J., Brochet, S., Dennetiere, D., and Polack, F., "Grating metrology for X-ray and V-UV synchrotron beamlines at SOLEIL," Rev. Sci. Instrum. 90(2), 021714 (2019). <https://doi.org/10.1063/1.5055284>.
[42] Siewert, F., Lammert, H., Reichardt, G., Hahn, U., Treusch, R., and Reininger, R., "Inspection of a spherical triple VLS-grating for self-seeding of FLASH at DESY," AIP Conf. Proc. 879, 667-670 (2007). <https://doi.org/10.1063/1.2436150>.
[43] Lin, S.-W., Wang, D.- J., Fu, H.-W., Tsai, H. M., Hua, C.-Y., Kuo, C.-Y., Hsu, M. -Y., Kao, K. -Y., Yin, G.-C., Fung, H.-S., Perng, S. -Y., Chang, C.-F., "Development of a long trace profiler in situ at National Synchrotron Radiation Research Center," Rev. Sci. Instrum. 90(2), 021716 (2019) <https://doi.org/10.1063/1.5055634>.
[44] Yashchuk, V. V., "Optimal Measurement Strategies for Effective Suppression of Drift Errors," Rev. Sci. Instrum. 80, 115101/1-10 (2009). < http://dx.doi.org/10.1063/1.3249559>.
[45] MÖLLER-WEDEL OPTICAL, GmbH, "ELCOMAT 3000." <https://www.haag-streit.com/moeller-wedel-optical/products/electronic-autocollimators/elcomat-series/elcomat-3000/>.
[46] Siewert, F., Noll, T., Schlegel, T., Zeschke, T., and Lammert, H., "The Nanometer Optical Component Measuring machine: a new Sub-nm Topography Measuring Device for X-ray Optics at BESSY," AIP Conf. Proc. 705, 847–850 (2004). < https://doi.org/10.1063/1.1757928>.
[47] Siewert, F., Buchheim, J., and Zeschke, T., "Characterization and calibration of 2nd generation slope measuring profiler," Nucl. Instrum. and Meth. A 616(2–3), 119-127 (2010). <https://doi.org/10.1016/j.nima.2009.12.033>.
[48] Siewert, F., Buchheim, J., Boutet, S., Williams, G. J., Montanez, P. A., Krzywinski, J., and Signorato, R., "Ultra-precise characterization of LCLS hard X-ray focusing mirrors by high resolution slope measuring deflectometry," Opt. Express 20(4), 4525-4536 (2012). <https://doi.org/10.1364/OE.20.004525>.
[49] Illemann, J., "Absolute high-accuracy deflectometric measurement of topography," Proc. SPIE 5188, 308-319 (2003). <https://doi.org/10.1117/12.507867>.
[50] Schulz, M., Ehret, G., and Fitzenreiter, A., "Scanning deflectometric form measurement avoiding path-dependent angle measurement errors," J. European Opt. Soc.: Rapid Publications 5, 10026 (2010). <https://doi.org/10.2971/jeos.2010.10026>.
[51] Ehret, G., Schultz, M., Stavridis, M., and Elster, C., "Deflectometric systems for absolute flatness measurements at the PTB," Meas. Sci. Technol. 23, 094007 (2012). <https://doi.org/10.1088/0957-0233/23/9/094007>.

[52] Yashchuk, V. V., Barber, S., Domning, E. E., Kirschman, J. L., Morrison, G. Y., Smith, B. V., Siewert, F., Zeschke, T., Geckeler, R., and Just, A., "Sub-microradian surface slope metrology with the ALS Developmental Long Trace Profiler," Nucl. Instr. and Meth. A 616(2-3), 212-223 (2010). <https://doi.org/10.1016/j.nima.2009.10.175>.
[53] Lacey, I., Artemiev, N. A., Domning, E. E., McKinney, W. R., Morrison, G. Y., Morton, S. A., Smith, B. V., and Yashchuk, V. V., "The developmental long trace profiler (DLTP) optimized for metrology of side-facing optics at the ALS," Proc. SPIE 9206, 920603 (2014). < https://doi.org/10.1117/12.2061969>.
[54] Alcock, S. G., Sawhney, K. J. S., Scott, S., Pedersen, U., Walton, R., Siewert, F., Zeschke, T., Senf, F., Noll, T., and Lammert, H., "The Diamond-NOM: A non-contact profiler capable of characterizing optical figure error with sub-nanometre repeatability," Nucl. Instr. Meth. A 616(2-3), 224-228 (2010). <https://doi.org/10.1016/j.nima.2009.10.137>.
[55] Assoufid, L., Brown, N., Crews, D., Sullivan, J., Erdmann, M., Qian, J., Jemian, P., Yashchuk, V. V., Takacs, P. Z., Artemiev, N. A., Merthe, D. J., McKinney, W. R., Siewert, F., and Zeschke, T., "Development of a high-performance gantry system for a new generation of optical slope measuring profilers," Nucl. Instrum. Meth. A 710, 31-36 (2013). < https://doi.org/10.1016/j.nima.2012.11.063>.
[56] Nicolas, J. and Martınez, J. C., "Characterization of the error budget of Alba-NOM," Nucl. Instr. and Meth. A 710, 24-30 (2013). <https://doi.org/10.1016/j.nima.2012.10.125>.
[57] Qian, S., Geckeler, R. D., Just, A., Idir, M., and Wu, X., "Approaching sub-50 nanoradian measurements by reducing the saw-tooth deviation of the autocollimator in the Nano-Optic-Measuring Machine," Nucl. Instr. and Meth. A 785, 206-212 (2015). <https://doi.org/10.1016/j.nima.2015.02.065>.
[58] Qian, S. and Idir, M., "Innovative nano-accuracy surface profiler for sub-50 nrad rms mirror test," Proc. SPIE 9687, 96870D (2016). <https://doi.org/10.1117/12.2247575>.
[59] Barber, S. K., Morrison, G. Y., Yashchuk, V. V., Gubarev, M. V., Geckeler, R. D., Buchheim, J., Siewert, F., and Zeschke, T., "Developmental long trace profiler using optimally aligned mirror based pentaprism," Opt. Eng. 50(5), 053601/1-10 (2011). <https://doi.org/10.1117/1.3572113>.
[60] Barber, S. K., Geckeler, R. D., Yashchuk, V. V., Gubarev, M. V., Buchheim, J., Siewert, F., and Zeschke, T., "Optimal alignment of mirror based pentaprism for scanning deflectometric devices," Opt. Eng. 50(7), 0073602-1-8 (2011). <https://doi.org/10.1117/1.3598325>.
[61] Debler, E. and Zander, K., "Ebenheitsmessung an optischen Planflächen mit Autokollimationsfernrohr und Pentagonprisma", PTB Mitteilungen Forschen + Prüfen, Amts und Mitteilungsblatt der Physikalisch Technischen Bundesanstalt, Braunschweig und Berlin, 89, 339-349 (1979).
[62] Geckeler, R. D. and Just, A., "Optimized use and calibration of autocollimators in deflectometry," Proc. SPIE 6704, 670407/1-12 (2007). <https://doi.org/10.1117/12.732384>.
[63] Lacey, I., Anderson, K., Geckler, R. D., Just, A., Smith, B. V., and Yashchuk, V.V., "Transfer of autocollimator calibration for use with scanning gantry profilometers for accurate determination of surface slope and curvature of state-of-the-art x-ray mirrors," Abstract to SPIE Optics + Photonics 2019, Conference OP313: Advances in Metrology for X-Ray and EUV Optics VIII (San Diego, CA 11-15 August); tracking number: OP19O-OP313-30.
[64] Yashchuk, V. V., Irick, S. C., MacDowell, A. A., McKinney, W. R., and Takacs, P. Z., "Air convection noise of pencil-beam interferometer for long-trace profiler," Proc. SPIE 6317, 63170D/1-12 (2006). <https://doi.org/10.1117/12.681297>.
[65] Yashchuk, V. V., "Sub-microradian surface slope metrology at the ALS Optical Metrology Laboratory and around the World," Oral presentation at the First Meeting on Development of a New Optical Surface Slope Measuring System - OSMS-I (ALS, Berkeley, March 26, 2010).
[66] Yashchuk, V. V., Rochester, S., Lacey, I., and Babin, S., "Beyond-resolution reconstruction of 1D surface slope topography based on measured instrument's transfer function," (in preparation).
[67] Müller, H., Böhm, G., and Arnold, T., "Next generation of a linear chirped slope profile fabricated by Plasma Jet Machining," Proc. SPIE 11171, 111710A (2019). <https://doi.org/10.1117/12.2526746>.
[68] Yashchuk, V. V., Centers, G., Tyurin, Yu. N., and Tyurina, A. Y., "Modeling surface topography of state-of-the-art x-ray mirrors as a result of stochastic polishing process: recent developments," Proc. SPIE 9962, 99620G (2016). <https://doi.org/10.1117/12.2238260>.
[69] Ralf D. Geckeler, private communication (November, 2006).
[70] Senba, Y., Kishimoto, H., Miura, T., and Ohashi, H., "Development of a long trace profiler at SPring-8 using a newly developed slope sensor," Proc. SPIE 9962, 996204 (2016). <https://doi.org/10.1117/12.2239394>.